EXCESS SAG
CAUSED BY ALUMINUM COMPRESSION
IN 'ACSR' CONDUCTORS

Peter Catchpole, P.Eng
POWER Engineers, Inc.

A View of Sag: Sag vs. Temperature Plot

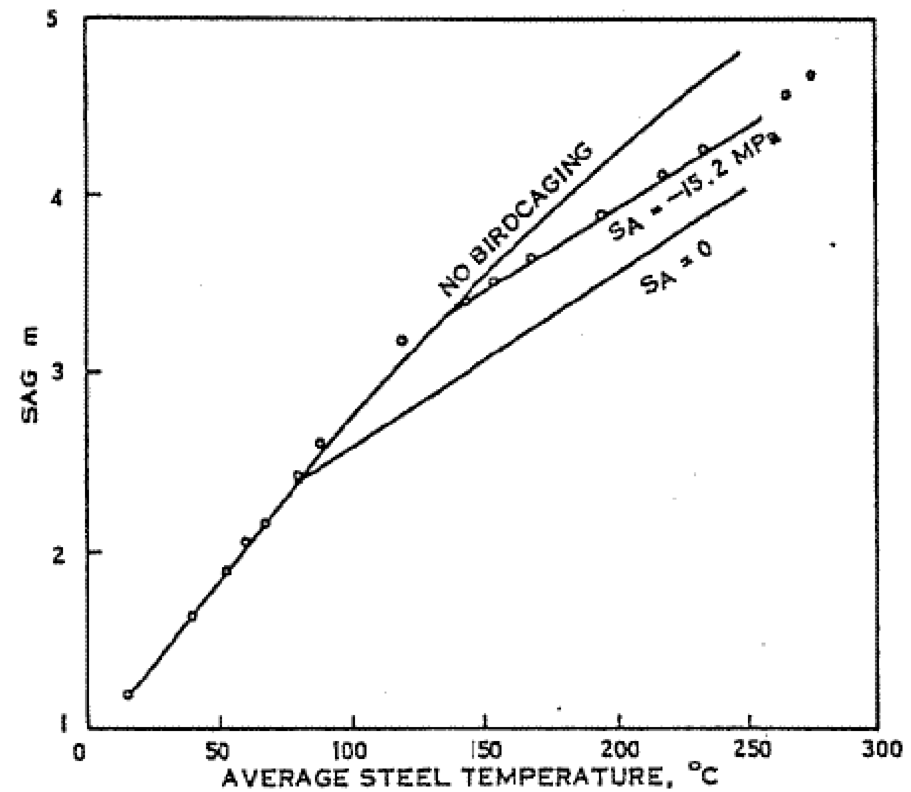

Figure 2: Measured and Calculated Sags of 2.78 cm (54/7) ACSR Conductor Pretensioned to 46.5 kN in a 122 m Span

S_A = stress in aluminum.

S_A = 0, no compression. This is how sag-tension programs "think."

No Birdcaging. IE: $S_A = \infty$

At S_A = -15 MPa, Sag error from Sag-tension Program in about 1 foot at all temperatures above the knee point.

A View of Stress-Strain

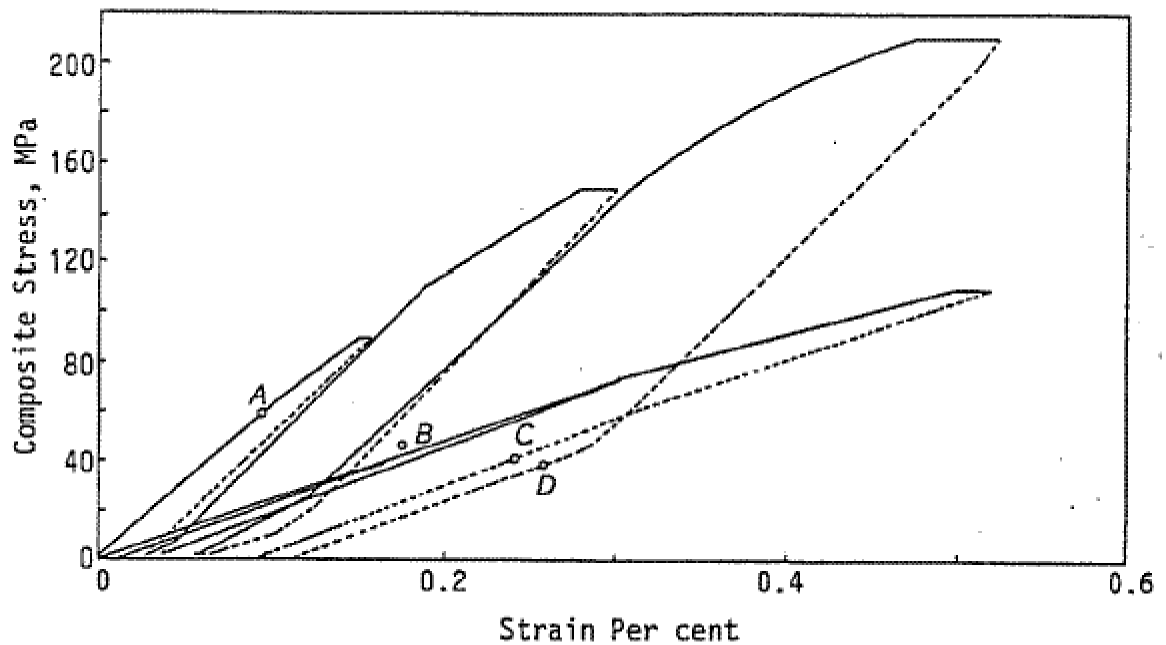

Figure: 14 Composite Stress-Strain Curve of 2.81 cm (26/7) ACSR Conductor and Reduced Stress of a New Steel Core of Conductor from the Same Reel

A: a point on the composite (core + Al) initial curve.

B: a point in the core initial curve.

C: A point on the core final curve.

D: A point on the composite final curve.

If there were NO compression stresses in the Al, C and D would be on the same line.

The C-D separation displays Al compression.

CEA Report 78-93

O. Nigol and J.S. Barrett
Ontario Hydro
Research Division
Toronto, Ontario

March, 1980

DEVELOPMENT OF AN ACCURATE MODEL OF ACSR
CONDUCTORS FOR CALCULATING SAGS
AT HIGH TEMPERATURES - PART I

Contract No 78-93

Ontario Hydro
Research Division

Report has three parts: I, II, III

Most of Parts I and II are provided to you as PDFs.

Report produced a new Sag-Tension computer program, STESS.

STESS was written to explore the compressed aluminum characteristic of ACSR.

The Compression Principle

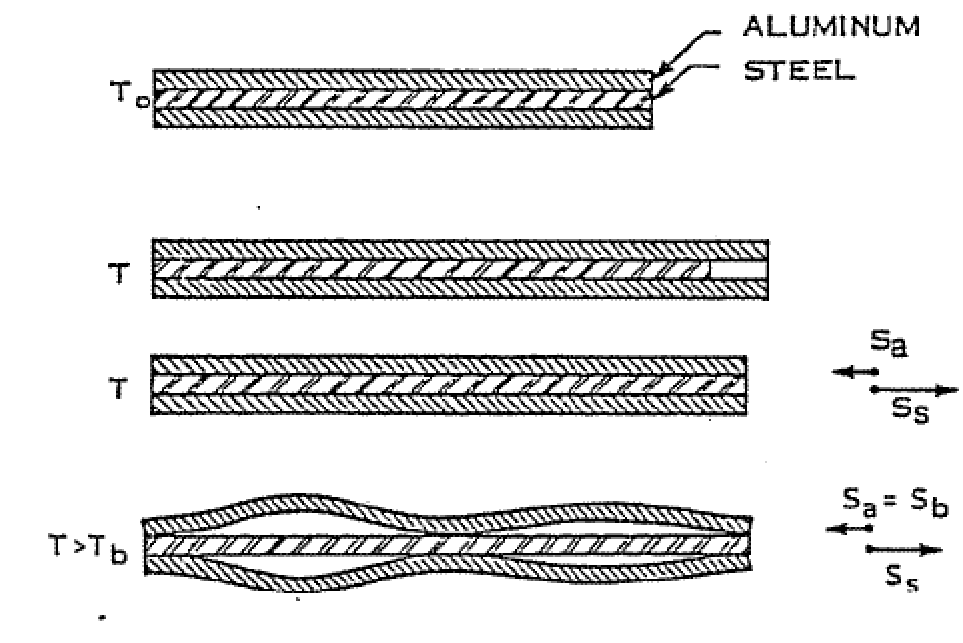

Figure 1: A Simple Thermal Model of ACSR Conductors

Top: at some temperature, the Al and core are the same length.

2nd: With heat applied, the Al expands “more” than the core.

3rd: BUT, the two metals are locked together at suspension clamps and dead ends causing Al compression and an equal tension in the core.

Bottom: If pushed hard enough, the helical Al strands (columns) will collapse (birdcage). IE: they do NOT carry infinite stress.

CEA Report Conclusion

CONCLUSIONS

Stress-strain and thermal elongation tests have demonstrated that the aluminum wires in ACSR conductors can support compressive stresses in the range from 6 MPa to 12 MPa. There is evidence from outdoor sag-temperature tests that the radial thermal gradients in the conductor, caused by wind, can increase the limiting compressive stress to 18 MPa or higher. This latter value of stress can account for excess high-temperature sags of roughly 1.5 m in a typical 300 m long span. Since the most critical high-temperature sags occur when there is little wind, a reasonable value of limiting compressive stress on aluminum to be used in sag-tension calculations is 10 MPa.

The large variance (6 to 12 MPa) is largely attributed to the variances in conductor design (layers and lay lengths), manufacturing variances (loose or tight stranding).

In other words, these are things beyond your control of your knowledge on a reel-for-reel basis. Therefore, approximating at 10 MPa (1,450 psi) is the best you can know.

But Chuck does not agree…

In the Report titled:

"Assessment of the Nigol-Barrett Theory of Compression Stress in the Aluminum Part of ACSR Due to Maximum Loading"

C. B. Rawlins (Chuck!)

The "aluminum compression" values obtained "by the calculations herein" are shown in MPa in the table below for the 26/7 and several other strandings.

Stranding	50% RS Max	70% RS Max
18/1	0.29	0.51
26/7	0.33	0.56
30/7	0.36	0.58
45/7	0.43	0.70
54/7	0.41	0.66
84/19	0.37	0.76

All values are far smaller than the CEA's 6 to 12 MPa

… the …CEA… rationale is qualitatively sound. However, the values… are insignificant and can have no practical impact in sag tension behavior.

What Does Chuck Say?

602 IEEE Transactions on Power Delivery, Vol. 14, No. 2, April 1999

Some Effects of Mill Practice on the Stress Strain Behavior of ACSR

Charles B. Rawlins, Fellow, IEEE
Alcoa Fujikura Ltd.
Brentwood, TN 37027

temperatures for overhead lines have increased, and two test programs, aimed at investigating effects of this increase, have revealed disparities between measured sags and those predicted by conventional sag tension calculations. The disparities are associated with high conductor temperatures. One program was carried out by Ontario Hydro [2,3], and the other by EPRI [5].

Alcoa Fujikura Ltd. commissioned the investigation reported here to identify the sources of these disparites. Among other possible sources, the influence of cable mill practices was studied, and it was concluded that variations in those practices may explain the deviant sags.

Two mill effects seem to stand out. One is associated with the presence of tensile stress in the aluminum part of ACSR, as it is placed on the reel. The other arises from variations in lengths of lay, permitted under ASTM standards [7].

Stranding Practices

It happens that essentially all multilayer ACSR manufactured in the US before WWII was stranded in one pass. This was also the period when stress strain curves for the standard strandings were established. At that time, a stress-free conductor was considered normal and desirable, and standard stress strain curves were constructed assuming that condition. That assumption became the default industry standard, and appears to be even to this day.

After WWII, and especially after 1950, two-pass stranding came increasingly into use because it afforded some cost savings in manufacture. Even though two-pass ACSR was often visibly not stress-free, stress strain curves were still constructed on the stress-free assumption. This

For example…

final curve. We conclude that the cable used in the test was stranded and put on the reel with built-in aluminum stress of at least 9.6 MPa (1400 psi) virtual, or over 11 MPa (1600

These stresses are in the right ballpark for compatibility with the CEA report.

How clear-cut is the issue?

> The built-in stress values obtained, before and after WWII, reflect the shift from one- to two-pass stranding. Out of thirty-nine tests of multilayer ACSR before the war, where the data permitted its estimation, only two showed significant built-in stress. Post-war, of fifty-two such tests, twenty showed built-in stress.

Pre-War: 2 or 39 samples showed pre-stress

Post-War: 20 or 52 samples showed pre-stress
(includes some pre-War samples)

Other Contributing Factors

- Modulus of Elasticity changes with:
  - Lay Length of layer
  - Temperature
  - Whether in tension or compression

> [redacted] Because of the limited amount of data available, and the large amount that would be required to do it, it seems unlikely that these effects can feasibly be sorted out and evaluated separately in the foreseeable future.

Chuck’s Stress-Strain Plot

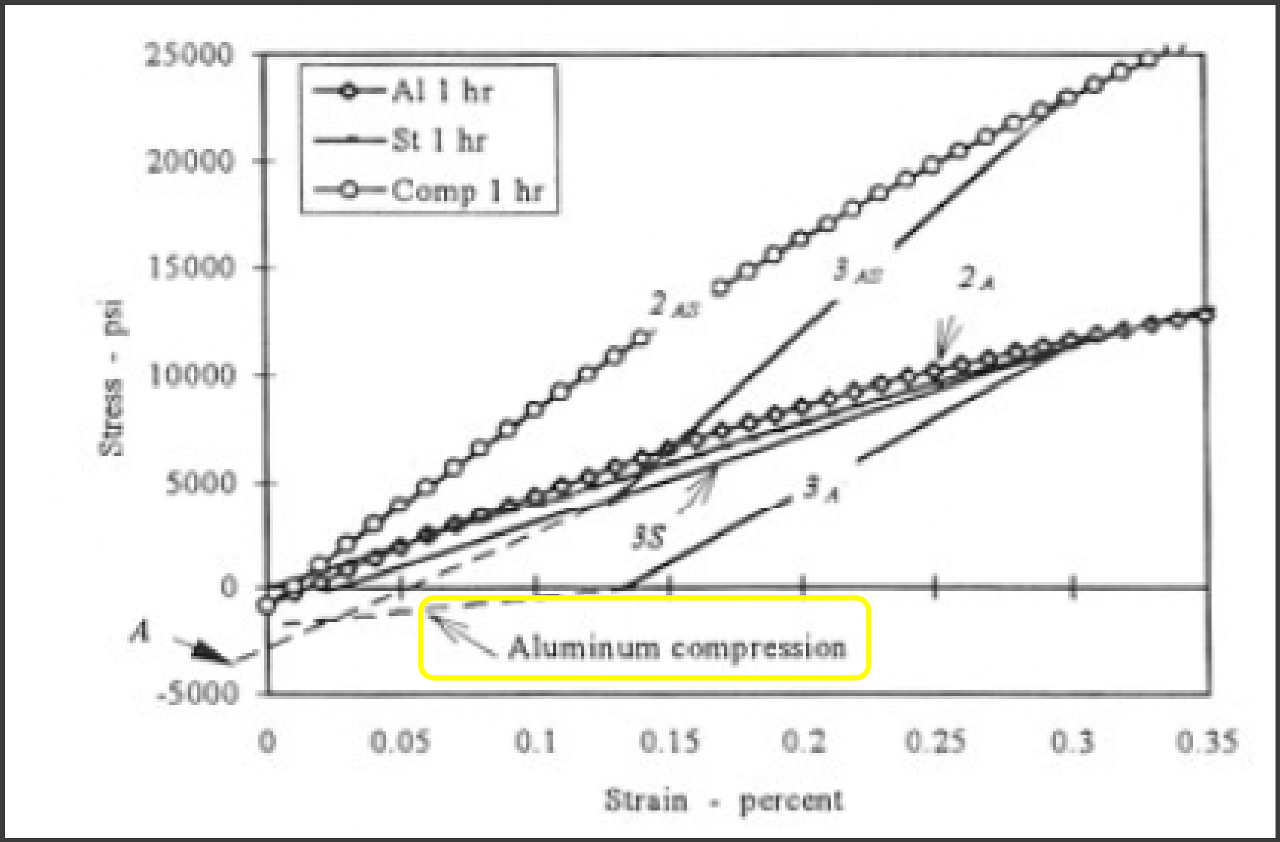

Notice that the compression creates a final, high temperature curve of a new slope rather than offset and parallel as CEA reported.

Chuck's Sag-Temperature Plot

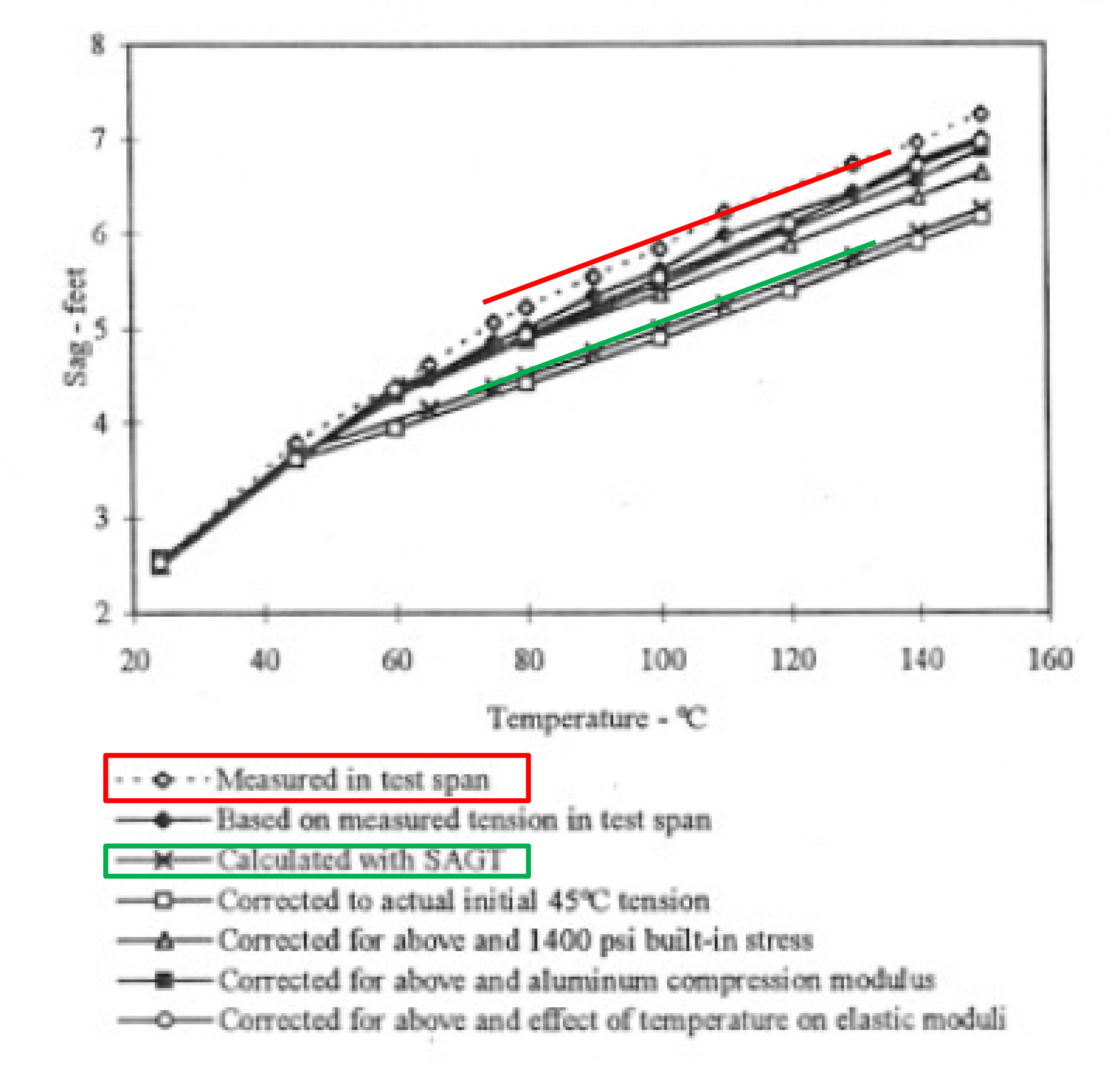

Notice that the computer program under states the test-measured sag by about a foot.

All of the intermediate plots are factors that try to account for the difference, as per Chuck.

Chuck’s Conclusion

> [redacted] we feel that the effects of built-in stresses and finite aluminum compression modulus largely account for the disparity turned up by the EPRI test. Our conclusion is that provision for taking these mill effects into account in sag tension calculations is appropriate.

Chuck is pretty adamant that his understanding of the sources of aluminum compression are correct and that the CEA report is wrong.

Despite the difficulty in learning more, as noted in his work, our industry should consider putting effort into the subject sometime. Until then, we have these two sources of information “out there” without a discerning opinion having been sought.

My Conclusions – as a line engineer

- Things have changed, as Chuck noted.
  - We make the wires differently since the 50s
  - Our analysis method is computerized but not updated to account for the fact that…
  - We use the wires differently (hotter) and are in uncharted territory relative to the method.
- Wires are more complicated than our model.
- Wires characteristics are more variable that we will ever track.
- Therefore…
  - Account for the understated sag as best you can.

Sadness Reigns

Free Market competition trumps Technology

- STESS is a great computer program
  - that will never see the light of day.
- SAG10 is a pretty good program
  - that will see limited use
- PLS-CADD owns the market with its *integrated* sag-tension module.

In SAG10 (Alcoa's program, now with Southwire)

- You can, as an option account for aluminum compression and generate the excess sag at higher temperatures
- The program does so in full compliance with Chuck's work, as presented here.

In PLS-CADD…

- You can set the compression limit to whatever you like.
  - The model mimics the CEA mechanics.
  - As of version 9.30, there are two input locations. The default value in one location is “infinity” and that overstates HT sag as much as can be done. Change that!
  - Since the compression limit… OR IS IT..
  - Since the built-in stresses are highly variable (0 to 12 MPa, 18?) and so on, consider this…

Aristotle said… (so they say. I wasn't there)

"It is the mark of an instructed mind to rest satisfied with the degree of precision which the nature of the subject admits and not to seek exactness when only an approximation of the truth is possible."

If we listen to Aristotle…

- Do NOT sweat the details of what the limit is. Use 1.5 Ksi to be conservative or 1.2 Ksi to be less conservative.
  - You are arguing over less than 1 foot of sag with your choice and you will NEVER predict reality better than that with hot ACSR.
- BTW… this behavior should apply to any bi-material conductor, not just to ACSR.
  - However, the degree of compression will arguably vary depending on the cause of the behavior – because that is still unresolved.

Assessment of the Nigol-Barrett Theory of Compression Stress in the Aluminum Part of ACSR Due to Maximum Loading

C. B. Rawlins

Introduction

In his written discussion of Rawlins' IEEE paper on mill effects [1], Dr. Barrett gives the most extensive statement yet of the suggested source of compression stress in the aluminum of ACSR [2]:

"The inner aluminum layer has a smaller lay angle than the outer layer. My detailed model shows that this results in a higher elastic modulus and higher stress on the inner layer under most conditions. This, in turn, results in larger permanent elongation of the inner layer during prestress or creep. The inner layer therefore normally 'goes slack' before the outer layer upon approaching birdcaging situations."

This description is of interest because it offers justification for the existence of compressive stress in the aluminum in the slack aluminum leg of the final stress strain curve of ACSR following loading to a high tension. This compressive stress, σ_{AK}, is shown in Fig. 1. It comes about, during unloading from maximum tension, when the net tension in the aluminum reaches zero (at ε_P) before the pressure of the aluminum layers on the core reaches zero (at ε_F). When that pressure passes through zero the aluminum part of the conductor becomes free to dilate away from the core and the aluminum incremental modulus changes from a high value to a quite low one. The knee point of the final stress strain curve occurs at this point. Dr. Barrett's statement seeks to explain why $\varepsilon_F < \varepsilon_P$.

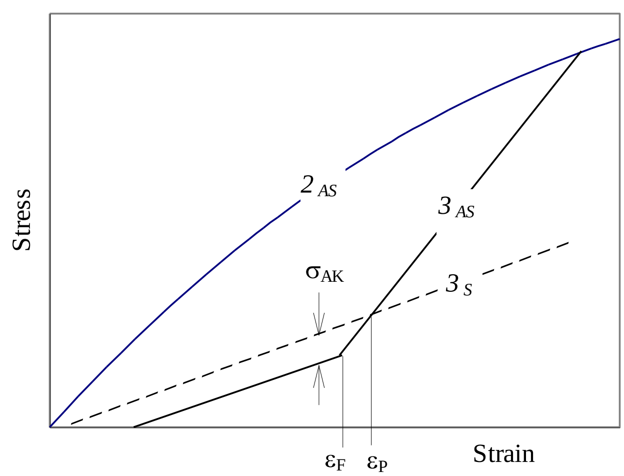

Fig. 1 Compression in aluminum in final composite stress strain curve

Explanation of Separation of Kneepoint from Zero Tension Point

The essence of Dr. Barrett's explanation is that the inner aluminum layer or layers experience greater plastic strain during high tension loading of the conductor than the outer layer because the inner layers have shallower angles of lay than the outer. The greater plastic strain of the inner layer causes it to have less stress when the strain in the conductor is reduced. The inner layers are then forced into compression when they pass zero stress because the outer layer is still in tension and constrains the inner layers from expanding radially.

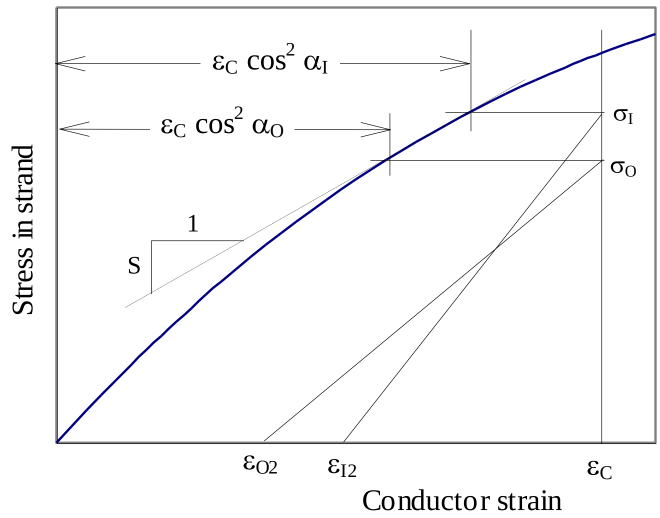

Fig. 2 Stresses and strains in inner and outer layers

This argument can be put in quantitative terms by reference to Fig. 2, which pertains to a conductor having two aluminum layers. The curve is the initial stress strain curve for an aluminum strand. Now, if the conductor is strained to ε_c, the strands of the inner and outer layers will also be strained. However, they will not be strained as much as the conductor. As shown in Fig. 3, the arc length of a helix is greater than that of its axis by the factor $l/\lambda = 1/\cos\alpha$; and only one component, proportional to $\Delta l/\Delta\lambda = \cos\alpha$, of the conductor's strain is directed along the strand's axis. Thus the strain experienced by the strand is only $\varepsilon_c \cdot \cos^2\alpha$. These strains for the inner and outer layers are shown in the Fig. 2, where the subscripts *I* and *O*, respectively, apply. The stresses in the two layers at maximum load are therefore σ_I and σ_O in Fig. 2.

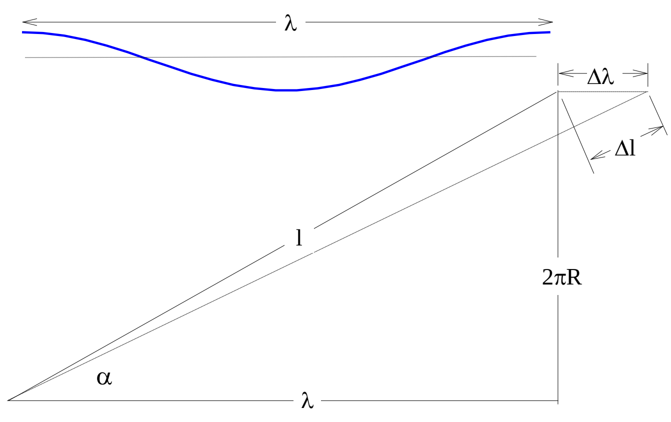

Fig. 3 Resolution of strains in helical strand

When the load is reduced, the stresses in the two layers follow their respective final moduli down, reaching zero stress at ε_{I2} and ε_{O2}. These final moduli are $E \cdot \cos^2 \alpha_I$ and $E \cdot \cos^2 \alpha_O$. Obviously,

$$\varepsilon_{I2} = \varepsilon_c - \frac{\sigma_I}{E \cos^2 \alpha_I} \qquad \varepsilon_{O2} = \varepsilon_c - \frac{\sigma_O}{E \cos^2 \alpha_O} \tag{1}$$

Now, the strains that occur on the initial loading produce plastic deformation, as reflected in the fact that the slope of the initial curve is less than *E* in the vicinity of σ_I and σ_O. If we call this slope *S*, then the difference between σ_I and σ_O is,

$$\sigma_I - \sigma_O = S\varepsilon_c \left(\cos^2 \alpha_I - \cos^2 \alpha_O \right) \tag{2}$$

Thus if we assume values for σ_I, ε_c, *S* and the lay angles, we can calculate ε_{I2} and ε_{O2}.

We are interested in the values of ε where the net aluminum tension and net inward gripping force from the aluminum each reach zero. Under final conditions, the layer modulus, referred to the conductor, is $E \cdot \cos^3 \alpha$. Thus, the components of stress in the aluminum layers *in the direction of the conductor axis* are,

$$\sigma_I = E \cdot \cos^3 \alpha_I \left(\varepsilon - \varepsilon_{I2} \right) \qquad \sigma_O = E \cdot \cos^3 \alpha_O \left(\varepsilon - \varepsilon_{O2} \right)$$

These stresses are illustrated in the top panel of Fig.4.

The tensions in the aluminum layers in the direction of the conductor axis are given by,

$$\begin{aligned} P_I &= n_I A \sigma_I = n_I E A \cos^3 \alpha_I \left(\varepsilon - \varepsilon_{I2} \right) \\ P_O &= n_O A \sigma_O = n_O E A \cos^3 \alpha_O \left(\varepsilon - \varepsilon_{O2} \right) \end{aligned} \tag{3}$$

We can solve (3) simultaneously for the value of ε where $P_I + P_O = 0$; the result, ε_P, is the conductor strain where net aluminum tension vanishes, as illustrated in the second panel of Fig. 4.

The inward pressure exerted by a helical strand due to its tension is equal to its tension *T* times the inward curvature of the helix, κ, per unit length of strand, where $\kappa = \sin^2 \alpha / R$. Thus, the inward force by the entire layer per *conductor* unit length is,

$$F = \frac{nT}{\cos \alpha} \kappa = \frac{P}{\cos^2 \alpha} \kappa = nEA \frac{\sin^2 \alpha \cdot \cos \alpha}{R} \left(\varepsilon - \varepsilon_2 \right) \tag{4}$$

This applies with appropriate subscripts to each layer. We can solve for the ε where $F_I + F_O = 0$, as illustrated in the third panel of Fig. 4. The result, ε_F, is the conductor strain where the grip by the aluminum on the core vanishes.

The strains ε_P and ε_F necessarily fall between ε_{I2} and ε_{O2}. In general, the lay angle in the outer layer is greater than in the inner. When that is true, $\varepsilon_P > \varepsilon_F$, so zero tension is reached before the kneepoint, as illustrated in Fig. 1, and the virtual stress in the aluminum at the knee point is,

$$\sigma_{AK} = H_A E_A \cdot \left(\varepsilon_F - \varepsilon_P \right) \tag{5}$$

where E_A is the final aluminum modulus (true, not virtual) and H_A is the aluminum fraction of the total conductor area. Aluminum compression occurs when $\varepsilon_P > \varepsilon_F$.

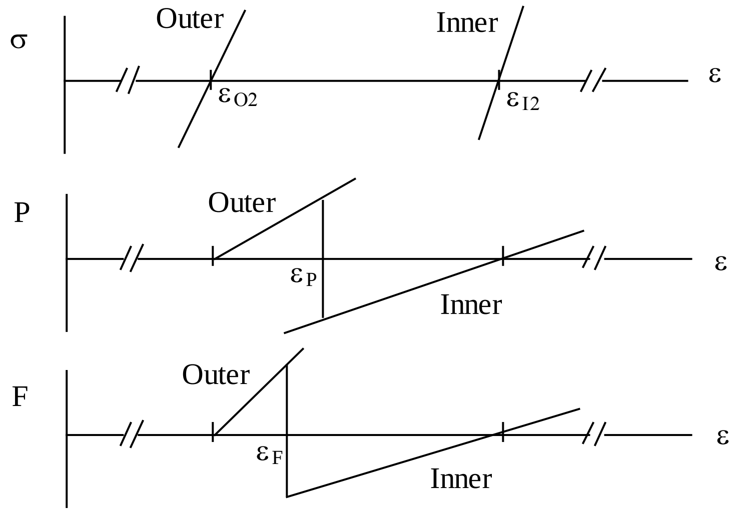

Fig. 4 Determination of zero aluminum tension and zero force on core

Magnitudes of Aluminum Compression Stresses

Equation (5) has been evaluated for reasonable values of input parameters, assuming the combinations of lay angles within ASTM limits that cause the greatest compressive stress. For the 26/7 stranding, the input parameters were:

Max. Tension	50% RS	70% RS
ε_c	0.0027	0.0045
σ_I (MPa)	121	145
S (MPa)	22410	8960
E (MPa)	68950	68950

The values of σ_I and S were read from a typical stress strain test of a 1350H19 aluminum strand. The values of σ_{AK} obtained are shown in MPa in the table below for the 26/7 and several other strandings.

Table I

Stranding	18/1	26/7	30/7	45/7	54/7	84/19
50% RS Max	-0.29	-0.33	-0.36	-0.43	-0.41	-0.37
70% RS Max	-0.51	-0.56	-0.58	-0.70	-0.66	-0.76

When the outer layer lay ratio was increased from its minimum of 10 to the preferred value of 11, σ_{AK} was almost halved in all cases shown in the table. The compressive stresses displayed in the table are clearly quite small. For practical purposes, ε_P and ε_F are congruent.

If the above analysis reads Dr. Barrett's rationale correctly, then the rationale is qualitatively sound. However, the values of σ_{AK} that it predicts are insignificant and can have no practical impact in sag tension behavior.

Effect of Radial Strains of Aluminum Layers

The analysis above ignores effects of radial contraction and expansion of the conductor as it is stretched and unstretched. These effects increase the separation $\sigma_I - \sigma_O$ and decrease the final moduli of Fig. 2. As a result, they make ε_F more positive relative to ε_P. That is, they reduce (and generally eliminate) the aluminum compressive stress at the knee point. Therefore, (5) puts an upper limit on the magnitude of compressive stress.

The following discussion describes the effects of radial strains in more detail.

Radial strains occur basically because the interface between a strand layer and the layer below it is springy. The contacts between layers are concentrated in small discrete elliptical areas where the strands from adjacent layers cross. When the conductor is tensioned, each layer presses against the layer below. This pressure is transmitted through the small contact areas, and, because they are small and not very numerous, the bearing stresses are high and significant strains and normal deformations take place around them.

On the initial loading, the contact stresses are large enough to cause significant plastic strain. When the tension is then reduced, the contacts behave elastically. Thus, the outward radial deflections on unloading are smaller than the inward deflections during initial loading. We will designate the inward initial deflections as $\delta_1 R$ and the unloading outward deflections as $\delta_2 R$. $\delta_1 R$ is always negative, and $\delta_2 R$ always positive.

Radial strains associated with Poisson's ratio also occur, but are smaller than those caused by normal compliance at the interlayer contacts.

Fig. 5

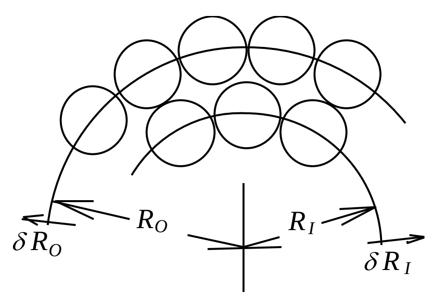

If the radial strains are superimposed on the longitudinal strains in the loading - unloading cycle, there are additional strains in the strands of the two layers. Since (see Fig. 3),

$$l = \sqrt{\lambda^2 + 4\pi^2 R^2} \tag{6}$$

the rate of change of the strain in a strand with respect to radial change is,

$$\frac{dl/l}{dR} = \frac{\sin^2 \alpha}{R} \tag{7}$$

Thus, the radial strain e_r is,

$$e_r = \frac{\delta l}{l} = \frac{\sin^2 \alpha}{R} \cdot \delta R \tag{8}$$

where δR is the change in the radius of the layer at the strand centerline. On initial loading, δR is negative (inward) and the layer strain is reduced by e_r. On unloading, it is increased by e_r. The particular values of e_r depend upon the layer α and R, and on the applicable δR, so the inward and outward values of e_r are generally different.

We can trace the effects of radial strains in Fig. 6, where we focus on one of the layers. The added strain on loading changes the value of σ_I or σ_O in Fig. 2. The Fig. 2 value, without radial strain, is labeled σ_A. According to (8), this shifts the stress to σ_B, for a net change of

$$\sigma_B - \sigma_A = \Delta_r\sigma = S \cdot e_r = S \cdot \frac{\sin^2\alpha}{R} \cdot \delta_1 R \tag{9}$$

This change results in a shift in ε_2 because the vertical fetch of the unloading leg is reduced. Since the modulus of the unloading leg is $E \cdot \cos^2\alpha$, the increment in ε_2 is

$$\Delta_{r1}\varepsilon_2 = \varepsilon_{2B} - \varepsilon_{2A} = -\frac{\Delta_r\sigma}{E \cdot \cos^2\alpha} = -\frac{S}{RE}\tan^2\alpha \cdot \delta_1 R \tag{10}$$

Note that ε_2 moves positive when $\Delta_r\sigma$ moves negative, which happens when $\delta_1 R$ is negative, i. e., inward.

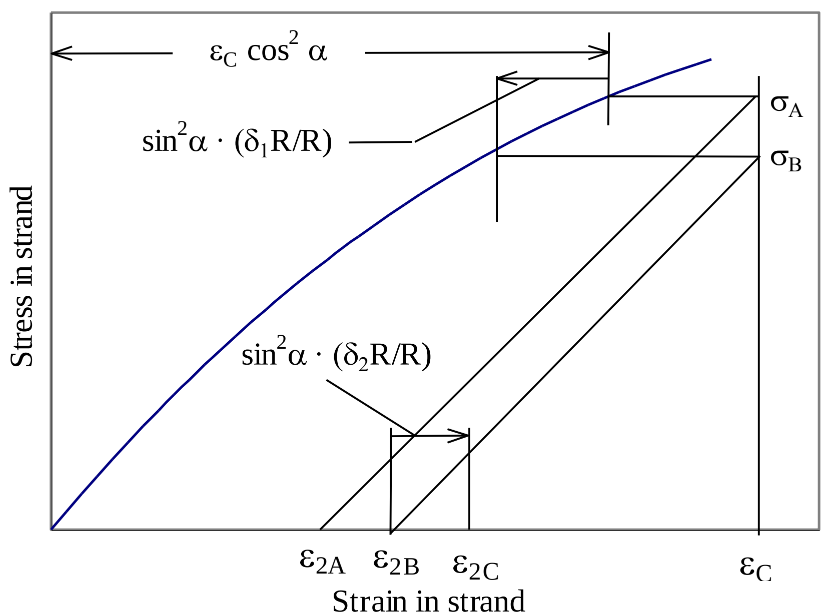

Fig. 6 Effects of Radial Strains in Nigol/Barrett Theory

The shift in ε_2 due to radial expansion on unloading, $\delta_2 R$, is simply

$$\Delta_{r2}\varepsilon_2 = \frac{\sin^2\alpha}{R} \cdot \delta_2 R \tag{11}$$

The net effect of radial strains on loading and unloading is

$$\Delta_{r1}\varepsilon_2 + \Delta_{r2}\varepsilon_2 = -\frac{S}{RE}\tan^2\alpha\cdot\delta_1 R + \frac{\sin^2\alpha}{R}\cdot\delta_2 R$$

$$= -\frac{\sin^2\alpha}{R}\cdot\left[\frac{S}{E\cos^2\alpha}\cdot\delta_1 R - \delta_2 R\right] \tag{12}$$

This pertains to one layer. The net change in $\varepsilon_{I2}-\varepsilon_{O2}$ (see Fig. 4) is the net of (12) for the inner and outer layers, that is

$$-\frac{\sin^2\alpha_I}{R_I}\cdot\left[\frac{S}{E\cos^2\alpha_I}\cdot\delta_1 R_I - \delta_2 R_I\right] + \frac{\sin^2\alpha_O}{R_O}\cdot\left[\frac{S}{E\cos^2\alpha_O}\cdot\delta_1 R_O - \delta_2 R_O\right] \tag{13}$$

$\delta_1 R$ is always negative (inward) and $\delta_2 R$ is always positive (outward), so the terms in brackets must be negative. $\delta_1 R$ incorporates plastic deformation at interlayer contacts and strand settling, while $\delta_2 R$ reflects only elastic movements, so $\delta_1 R$ is much larger. The second term, for the outer layer, dominates the first, which pertains to the inner layer, for reasons given below. Thus, the net effect of the radial strains is to move $\varepsilon_{I2}-\varepsilon_{O2}$ in the negative direction, toward reversing the order shown in Figs. 2 and 4. That necessarily tends to move $\varepsilon_F-\varepsilon_P$ in the positive direction, which, through (5), moves σ_{AK} in the positive direction, out of compression and toward aluminum tension.

The second term in (13) dominates the first as a result of two facts. First, the lay angle for the outer layer is in general enough larger than the inner that $\sin^2\alpha_O / R_O > \sin^2\alpha_I / R_I$. Second, the radial movements of the outer layer, $\delta_1 R_O$ and $\delta_2 R_O$, are larger than those of the inner layer, $\delta_1 R_I$ and $\delta_2 R_I$ because the radial stiffness of the conductor decreases from the core outward.

There is very little actual test data on these radial movements, all of it limited to the outer layer. Those results are most conveniently expressed as the ratio of radial strain to longitudinal strain, $(\delta R / R)/(\delta\lambda/\lambda)$, which is rather similar to Poisson's Ratio. For inward initial strains, values for the ratio range from about –0.4 to –1.5, based on data in [3]. For outward final strains, radial to longitudinal strain ratios of about zero and –0.7 were reported in [3].

Taking an inward ratio of –0.4 and outward of zero, the maxima of the ranges from [3], assuming that the inner layer deflects radially half as much the outer, and employing (13) in (3), (4) and (5) above, the stress σ_{AK} for 26/7 ACSR in Table I changes from 0.56 MPa to 0.21 MPa compression at 70% RS. At 50% RS, ε_{O2} becomes greater than ε_{I2} (see Fig. 2), so the outer layer unloads first and thus does not restrain the inner layer expansion when it unloads. Instead, a slight chamfer occurs at the kneepoint. If ratios of radial to longitudinal strain nearer the middle of the ranges in [3] are used, the outer layer unloads first at all tensions. Thus it appears that, in general, effects of radial strains remove entirely the small compression stresses predicted by the Nigol-Barrett theory.

Nomenclature

A Cross sectional area of aluminum strand
E Young's Modulus of aluminum
e Longitudinal strain of aluminum strand along its axis
e_r Strain of aluminum strand due to change in radius of layer
F Radial force per unit length of conductor applied by a layer due to its own tension
H_A Aluminum area as a fraction of total conductor area
l Arc length of strand in one lay length
n Number of strands in layer
P Contribution of strand layer to conductor tension
R Radius of strand layer at strand axes
δR Increment in layer radius
Δ_r Increment (in stress or strain) due to change in radius of layer
S Local slope of initial stress strain curve of aluminum strand
T Tension in aluminum strand
α Lay angle
ε Conductor strain
ε_c Maximum conductor strain
ε_F Conductor strain on unloading where net radial force by aluminum on core is zero.
ε_P Conductor strain on unloading where net tension in aluminum is zero
κ Curvature of strand due to its helicity ( )
λ Lay length
σ Stress in aluminum
σ_{AK} Average compression stress in aluminum at kneepoint (See Fig. 1).

Other Variable Subscripts

A Stress or strain neglecting radial strains of conductor (See Fig. 6)
B Stress or strain accounting for radial strains of conductor on initial loading
C Strain accounting for radial strains during loading and unloading
I Inner aluminum layer
O Outer aluminum layer
1 During or resulting from initial loading to maximum load
2 During or resulting from unloading following maximum load

References

[1] Charles B. Rawlins, "Some Effects of Mill Practice on the Stress Strain Behavior of ACSR," IEEE Paper No. PE-325-PWRD-0-12-1997.
[2] J. Stephen Barrett, Discussion of [1].
[3] O. Nigol and J. S. Barrett, "Development of an Accurate Model of ACSR Conductors for Calculating Sags at High Temperatures," Ontario Hydro Research Division, CEA Contract No. 78-93, Part I, March 1980 and Part III, March 1982.

Massena, NY
March 27, 1998

Note on the Aluminum Compression Hypothesis

C. B. Rawlins, Consultant
Massena, NY

The hypothesis that the aluminum part of ACSR can experience significant compressive stress at the kneepoint of the final leg of the stress strain curve was described in [1]. The analytical basis for that hypothesis was examined in detail in the closure to [2] and found to justify only insignificant aluminum compressive stress, if any, at the kneepoint.

The only experimental evidence of aluminum compression at the kneepoint is found in Fig. 3 of [1], which shows results of stress strain measurements on five sizes of ACSR. In two of these tests there was detectable aluminum compression at the kneepoint, and in one of those the compression was significant. Although significant compression was indicated in another test, illustrated in Fig. 9 of [1], that indication was a result of arbitrarily positioning the initial curve for the steel core to pass through the origin of the plot.

The method for determining aluminum stress at the kneepoint in the tests of Fig. 3 of [1] was to cut the aluminum after the conductor had been brought to zero tension at the end of the test. This cutting relieved all stress in the aluminum. When that was done, the sample contacted, showing that the core had been under tension, and thus the aluminum under compression, prior to cutting, even though the total conductor tension was zero.

The division of stress that had existed at the kneepoint was then surmised by projecting the final stress strain curve for the steel core back up from its strain that existed following the cutting of the aluminum. This strain corresponded to true zero tension in the core, so projecting the final curve from that point would give a valid assessment of the core stress during the final leg of the composite conductor's stress strain curve. In two of the tests of Fig. 3 of [1], this final steel core curve passed above the kneepoint, indicating that there was compressive stress in the aluminum there.

However, this result appears to be due to the use of incorrect steel core stress strain curves. These curves were reportedly obtained by making a separate stress strain test on a new sample of core from the same reel of conductor. Close examination of the data in Fig. 3 of [1] indicates that this was not the case for the two tests that displayed detectable aluminum compression at the kneepoint. Since it was the final legs of the steel core curves that were plotted there, their slopes correspond to the final moduli of those cores. The slopes of the core curves for the two tests in question are outside the range for 7-strand cores, and correspond, rather, to single-strand cores.

The plots displayed in Fig. 3 of [1] came from a report to the Canadian Electrical Association of work performed under contract by the Ontario Hydro Research Division [3]. The plot showing significant aluminum compression at the kneepoint in [1] is a reduced copy of Fig. 26 of [3], which is attached here as Fig. A. The attached copy shows how the slope was determined, and lists the corresponding final modulus values, both reduced and true.

Note that the true modulus determined from Fig. A is within the range of Young's Modulus for A-galvanized EHS steel: 29 to 30 $\cdot 10^6$ psi (200 to 210 GPa). In fact, Fig. 41 of [3], which is attached here as Fig. B, shows the stress strain test of the center wire from the core of the ACSR in question, and its modulus is within 1% of the *core* modulus found in Fig. 26 of [3].

Stranded cores have moduli significantly smaller than the single-wire cores because of effects of the helical construction. For 7-strand cores, conductor manufacturers show modulus values in stress strain charts spanning the range 26.0 to 28.2 million psi with 27.4 average (179 to 194 MPa with 189 average), covering a number of ACSR sizes and strandings. Of more direct interest, however, is a test shown in Fig. 10 of [4] on the identical size and stranding as in Fig. A. That figure is shown here as Fig. C. The true final modulus scaled from this figure is 26.5 million psi (183 MPa), which is 10% less than was found for the core plotted in Fig. A. The latter was clearly not a stranded 7-strand core.

Utilizing the final modulus actually measured for the conductor represented in Fig. A, instead of what is apparently a single strand core curve, alters the conclusion to be drawn from the test. This is shown in Fig. D. The final core curve passes directly through the kneepoint, showing that the aluminum stress there was zero.

The situation was the same for the fourth test in Fig. 3 of [1], which is Fig. 29 of [3]. That test showed a slight aluminum compression at the kneepoint. The true modulus of the core turned out to be 30 million psi (208 MPa), as scaled from Fig. 29 of [3]. In contrast, Fig. 26 of [4] shows the complete stress strain test of the core from the same size conductor. There, the final core modulus was 25 million psi (172 MPa). Utilizing this modulus instead of the spurious core curve again eliminated the apparent compressive stress in the aluminum at the kneepoint.

Thus, when appropriate steel core final moduli are employed, all five of the tests in [1], to determine aluminum compression at the kneepoint, show that there is none.

The presence of compression in the aluminum *at zero tension* is explained by the fact that the aluminum compression modulus is not zero. This aspect was analyzed in [2], and is a separate issue from conditions at the kneepoint.

2001 January 3

References

[1] O. Nigol and J. S. Barrett, "Characteristics of ACSR Conductors at High Temperatures and Stresses," *IEEE Transactions on Power Apparatus and Systems*, Vol. PAS-100, No. 2, February 1981, pp. 485-493.

[2] Charles B. Rawlins, "Some Effects of Mill Practice on the Stress Strain Behavior of ACSR," *IEEE Transactions on Power Delivery*, Vol. 14, No. 2, April 1999, pp. 602-629.
[3] O. Nigol and J. S. Barrett, "Development of an Accurate Model of ACSR Conductors for Calculating Sags a High Temperatures," Contract 78-93, Part I.
[4] Ibid., Part III.

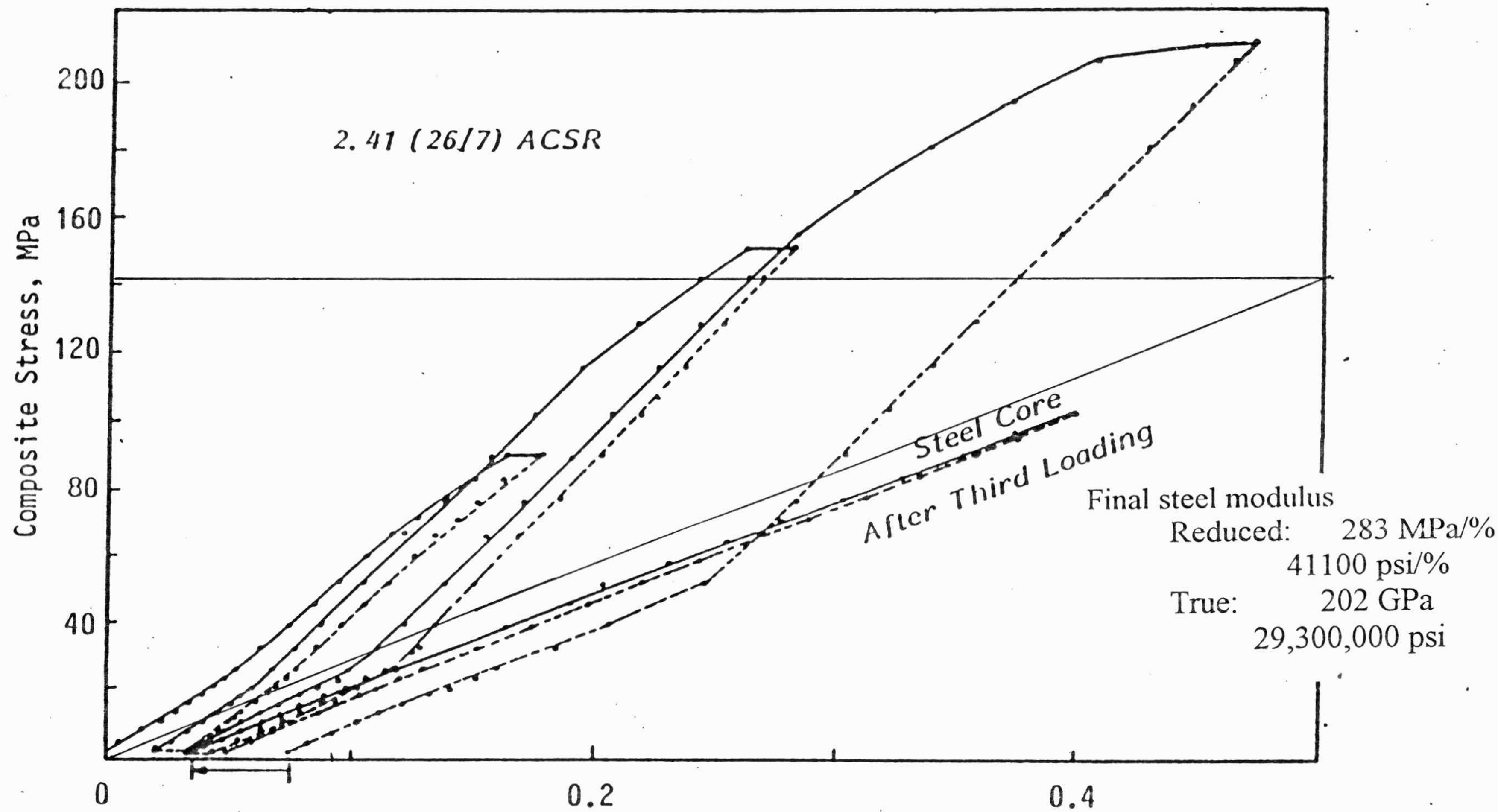

FIGURE 26
STRESS-STRAIN CURVES OF 2.41 cm (26/7) ACSR CONDUCTOR, MARCH 27, 1979

Figure A

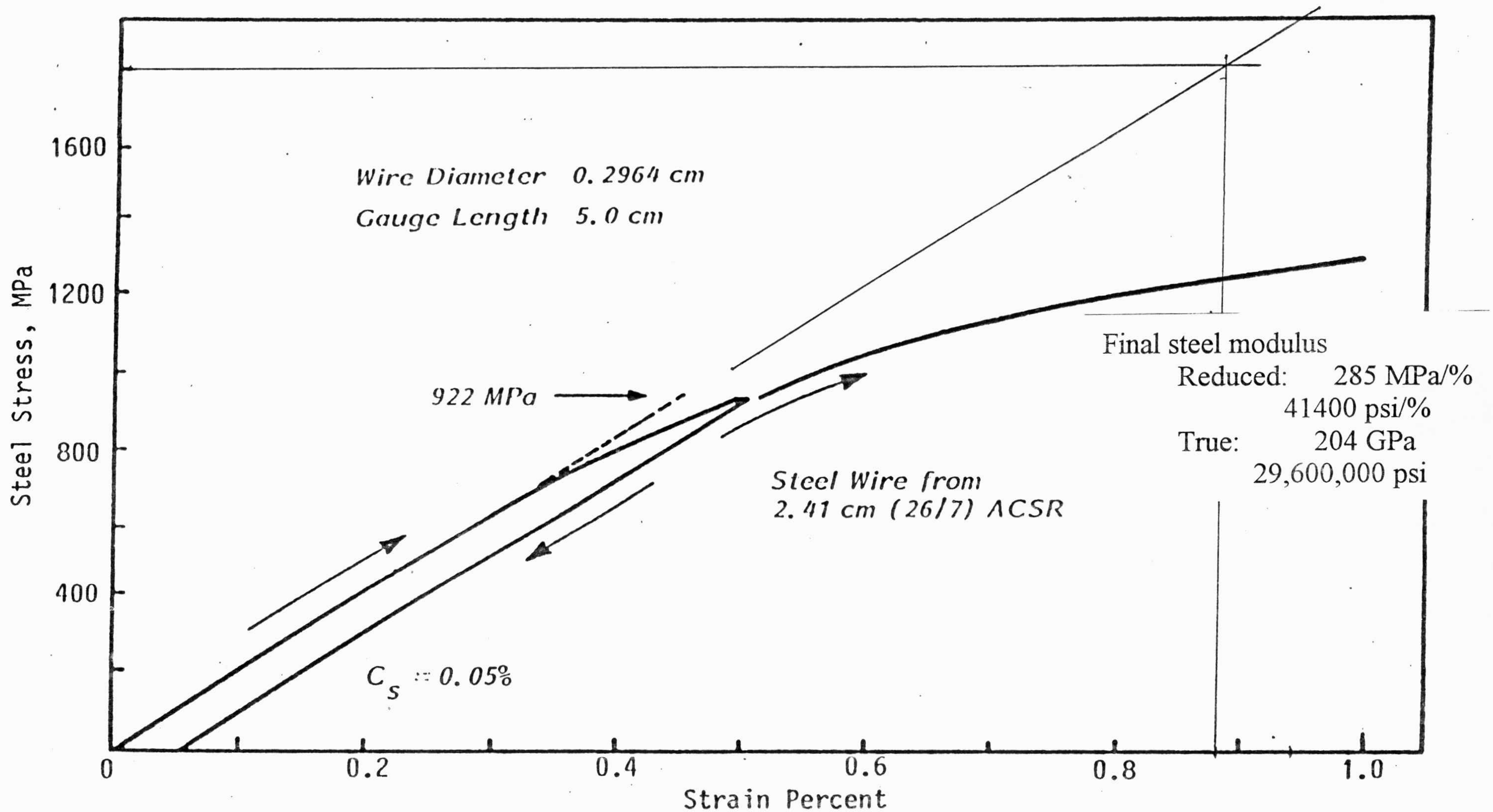

FIGURE 41

STRESS-STRAIN CURVE OF A STEEL KING-WIRE FROM 2.41 cm (26/7) ACSR CONDUCTOR

Figure B

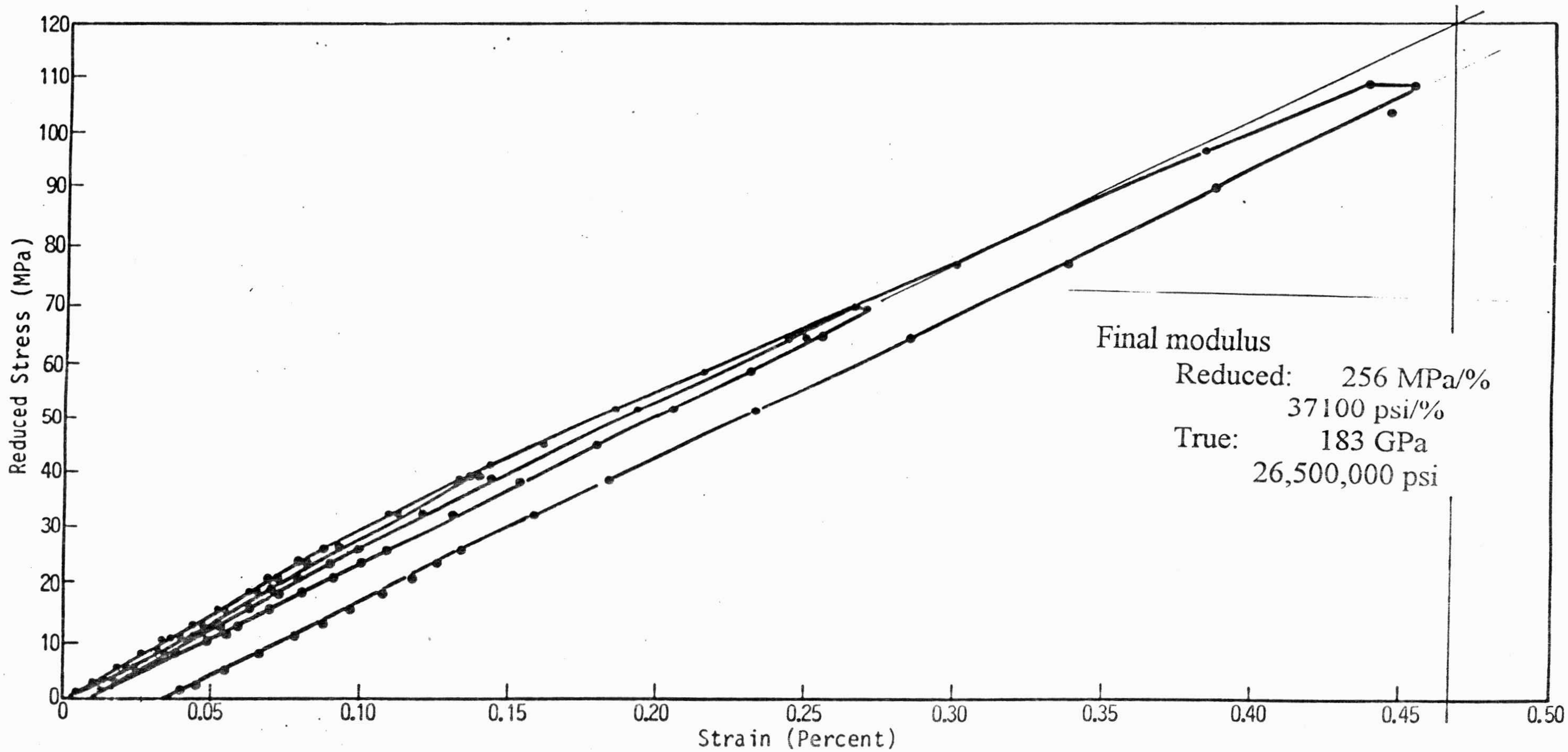

FIGURE 10

STEEL CORE OF 24.1mm (26/7) ACSR CONDUCTOR
JANUARY 13, 1981

Figure C

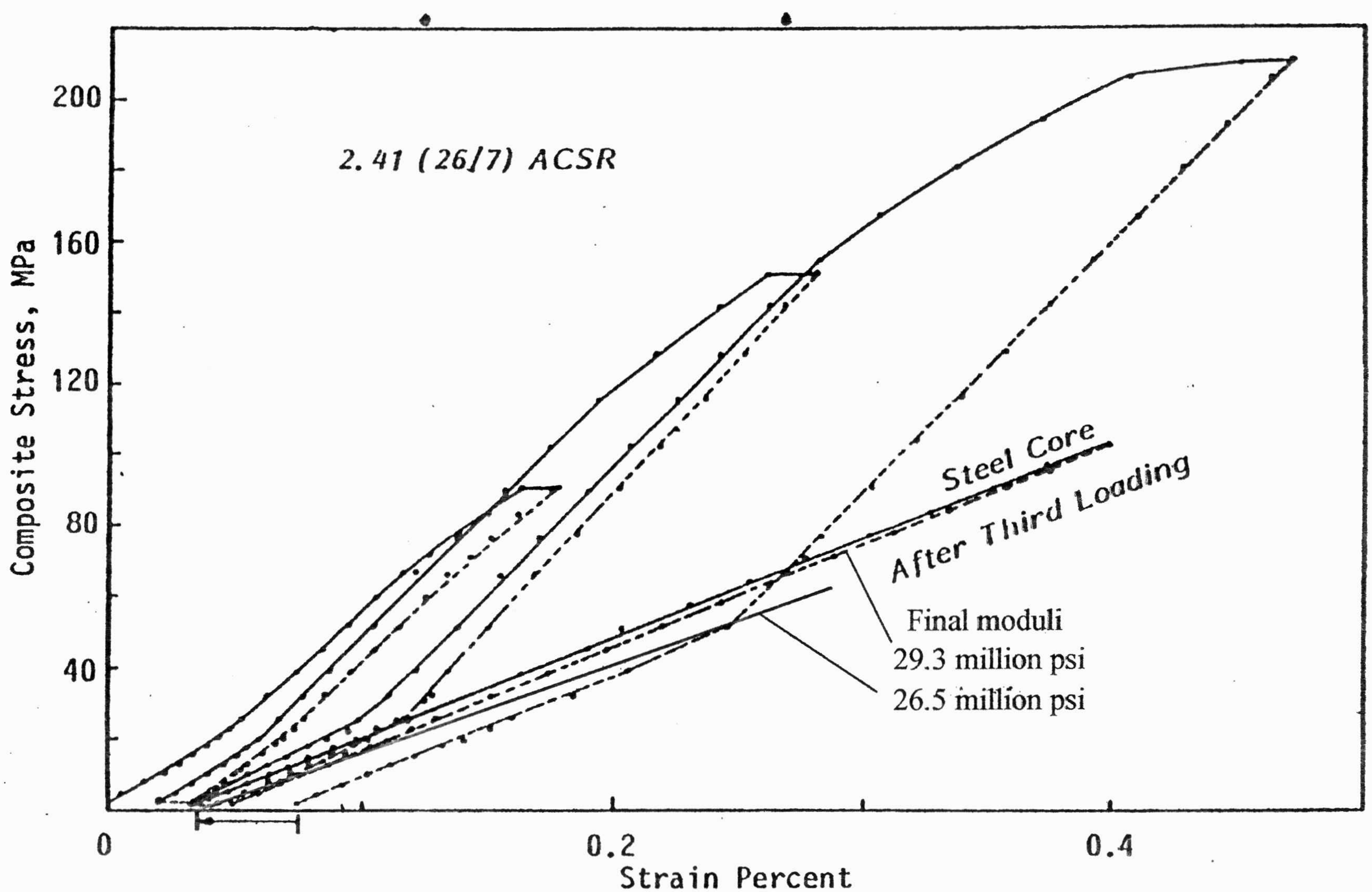

FIGURE 26

STRESS-STRAIN CURVES OF 2.41 cm (26/7) ACSR CONDUCTOR, MARCH 27, 197[illegible]

Figure D